ENVIRONMENTAL RESEARCH
LETTERS

PURPOSE-LED PUBLISHING™

LETTER • OPEN ACCESS

Spaceborne detection of XCO_2 enhancement induced by Australian mega-bushfires

To cite this article: Jun Wang *et al* 2020 *Environ. Res. Lett.* **15** 124069

Environmental Research Letters

LETTER

Spaceborne detection of XCO_2 enhancement induced by Australian mega-bushfires

Jun Wang[1,2,3], Zhiqiang Liu[4], Ning Zeng[2], Fei Jiang[1,3], Hengmao Wang[1,3] and Weimin Ju[1,3]

[1] International Institute for Earth System Science, Nanjing University, Nanjing, Jiangsu 210023, People's Republic of China
[2] Department of Atmospheric and Oceanic Science and Earth System Interdisciplinary Center, University of Maryland, College Park, MD 20742, United States of America
[3] Jiangsu Provincial Key Laboratory of Geographic Information Science and Technology, Key Laboratory for Land Satellite Remote Sensing Applications of Ministry of Natural Resources, School of Geography and Ocean Science, Nanjing University, Nanjing, Jiangsu 210023, People's Republic of China
[4] State Key Laboratory of Numerical Modelling for Atmospheric Sciences and Geophysical Fluid Dynamics, Institute of Atmospheric Physics, Beijing 100029, People's Republic of China

E-mail: wangjun@nju.edu.cn

Keywords: OCO-2 XCO_2 enhancement, Australian mega-bushfires, spaceborne detection, GEOS-Chem simulation

Supplementary material for this article is available online

OPEN ACCESS

RECEIVED
27 July 2020

REVISED
12 October 2020

ACCEPTED FOR PUBLICATION
6 November 2020

PUBLISHED
16 December 2020

Abstract

The 2019–20 Australian mega-bushfires, which raged particularly over New South Wales and Victoria, released large amounts of toxic haze and CO_2. Here, we investigate whether the resulting CO_2 enhancement can be directly detected by satellite observations, based on National Aeronautics and Space Administration's Orbiting Carbon Observatory-2 (OCO-2) column-averaged CO_2 (XCO_2) product. We find that smoke from wildfires can greatly obscure satellite observations, making the available XCO_2 mainly locate over outer fringes of plumes downwind of the major mega-bushfires in eastern Australia in three orbit observations during November–December 2019, with their enhancements of approximately 1.5 ppm. This fire-induced CO_2 enhancement is further confirmed using an atmospheric transport model, Goddard Earth Observing System-Chem, forced by satellite observation-derived fire product Global Fire Emissions Database, version 4.1 and wind observations, with comparable simulated XCO_2 enhancements. Model simulation also suggests that the sensitivity of the downwind maximum XCO_2 enhancement is 0.41 ± 0.04 ppm for 1 TgC d^{-1} fire emissions. In sum, though detectable to some extent, it remains a challenge to get the accurate maximum XCO_2 enhancements due to the gaps in XCO_2 detections obscured by smoke. Understanding the capability of OCO-2 XCO_2 detection is prerequisite for monitoring and constraining wildfire CO_2 emissions by inversions.

1. Introduction

The unprecedented 2019–20 Australian bushfires, which raged particularly over eastern Australia (the worst hit states were New South Wales and Victoria), drew worldwide attention. The worst fire incidents started at the beginning of November 2019. During November and December 2019, eastern Australia experienced record-breaking temperatures and widespread severe and extreme drought with decreased precipitation (supplementary figure 1 (available online at https://stacks.iop.org/ERL/15/124069/mmedia)), as indicated by previous studies (Boer *et al* 2020, Nolan *et al* 2020). This anomalous hot and dry climate may have been driven by natural atmospheric dynamics and anthropogenic global warming (Phillips and Nogrady 2020). The unusual positive Indian Ocean Dipole (IOD) in 2019 was one of the strongest such events in history. During the positive phase of IOD, decreased precipitation and warmer temperatures often occur over parts of Australia (Saji *et al* 1999, Saji and Yamagata 2003, Cai *et al* 2009). A sudden stratospheric warming above Antarctica can also cause the hot and dry conditions over Australia (Phillips and Nogrady 2020). These hot and dry conditions greatly contribute to catastrophic bushfires.

The mega-bushfires of 2019–20 burned vast areas of temperate broadleaf and mixed forests (Boer *et al* 2020, Nolan *et al* 2020). Approximately 5.8 million hectares were burned between September 2019 and early January 2020, accounting for around 21% of Australia's temperate broadleaf and mixed forests (Boer *et al* 2020). The fires greatly threatened the Gondwana Rainforests, a World Heritage site (Kooyman *et al* 2020). The fires caused losses of USD billions from the economy, as well as deaths of more than 30 humans and countless animals. Concurrently, the mega-bushfires released large amounts of toxic haze and CO_2, further threatening human health and contributing to the increase of global CO_2 concentrations.

Orbiting Carbon Observatory-2 (OCO-2) is the Earth remote sensing satellite used by National Aeronautics and Space Administration (NASA) to measure the atmospheric CO_2 concentration (Crisp *et al* 2008, Crisp and OCO-2 Team 2015). The OCO-2 column-averaged CO_2 (XCO_2) products have been used to detect the XCO_2 enhancement over both megacity and volcanoes (Schwandner *et al* 2017), analyze the variations of XCO_2 over the Niño 3.4 regions during the 2015–16 El Niño event (Chatterjee *et al* 2017), estimate the land–atmosphere carbon flux and fire emissions during the El Niño event (Heymann *et al* 2017, Liu *et al* 2017), and estimate the CO_2 emissions by megacities (Zheng *et al* 2020) and single power plants (Nassar *et al* 2017). In the previous study (Heymann *et al* 2017), the XCO_2 enhancement induced by fires was calculated as the difference between OCO-2 XCO_2 and background XCO_2 values on $0.5^\circ \times 0.5^\circ$ grids, where background XCO_2 was derived from a CO_2 model 'CarbonTracker' and observations unaffected by fires determined by the Stochastic Time-Inverted Lagrangian Transport model. In contrast, we in this study will investigate whether OCO-2 can directly and clearly detect the XCO_2 enhancement induced by Australian mega-bushfires, analogous to the study of Schwandner *et al* (2017), based on the combination of OCO-2 L2 XCO_2 product and Goddard Earth Observing System (GEOS)-Chem model simulations. Understanding the capability of OCO-2 to detect XCO_2 enhancement induced by eastern Australia's fires is important for monitoring and constraining wildfire CO_2 emissions over the whole of Australia.

2. Materials and methods

2.1. OCO-2 data

The space-based XCO_2 measurements used to detect XCO_2 enhancement in this study are retrieved from the OCO-2 mission (Crisp *et al* 2008, Crisp and OCO-2 Team 2015), which was launched into a near-polar orbit on 2 July 2014. The OCO-2 instrument has a narrow swath with the footprint <1.3 km $\times$ 2.25 km. Its retrieval algorithm was described by Crisp *et al* (2012) and O'Dell *et al* (2012). In this study, the XCO_2 retrievals are the version 9r level 2 product, which can be retrieved from the Goddard Earth Sciences Data and Information Services Center. Version 9r is the latest version of the XCO_2 dataset, containing bias-corrected XCO_2 and other selected fields. In this analysis, we used the good quality XCO_2 data, which were determined by the variable 'xco2_quality_flag' in the file.

2.2. Atmospheric transport model

The GEOS-Chem model version 12.5.0 (The International GEOS-Chem User Community 2019) was adopted in this study to simulate the XCO_2 enhancement induced by Australian bushfires. It is a global 3D atmospheric chemistry model driven by meteorological fields which are freely available at the GEOS of the NASA Global Modeling Assimilation Office.

Specifically, the driving meteorological fields and boundary carbon fluxes are as follows:

(a) The meteorological fields are the Modern-Era Retrospective analysis for Research and Applications, Version 2 (MERRA-2) (Gelaro *et al* 2017). MERRA-2 can utilize the newer microwave and hyperspectral infrared radiance observations, and is the first long-term global reanalysis to assimilate space-based aerosol measurements. In this study, we ran the GEOS-Chem model at the horizontal resolution of $4^\circ \times 5^\circ$ and 47 hybrid sigma-pressure levels up to 0.01 hPa. In addition, in the analysis, we further used its variables of surface air temperature, U and V winds at 940 hPa, and aerosol optical depth (AOD).

(b) The fossil fuel emissions are from the Open-Data Inventory for Anthropogenic Carbon Dioxide (ODIAC) which is a global CO_2 emission product from fossil fuel combustion (Oda and Maksyutov 2011, Oda *et al* 2018). In this study, we used the latest version of the ODIAC fossil fuel emission product 'ODIAC2019' with the original resolution of $1^\circ \times 1^\circ$ from 2000 to 2018. The emissions in 2019 are obtained by the linear extrapolation.

(c) The wildfire carbon emissions are based on the Global Fire Emissions Database, Version 4.1 (GFED4.1) (van der Werf *et al* 2017). This product was constructed by combining Moderate Resolution Imaging Spectroradiometer (MODIS) burned area maps with active fire data from the Tropical Rainfall Measuring Mission (TRMM) Visible and Infrared Scanner and the Along-Track Scanning Radiometer family of sensors. Satellite-based fire activity and vegetation productivity were combined to estimate gridded monthly fire emissions and scalars which can be used to derive higher temporal resolution emissions. It has the original horizontal

resolution of 0.25° × 0.25°. We distributed the monthly emissions into the daily values by use of the daily fraction variable (Mu *et al* 2011). However, as for the diurnal cycle, in this study we uniformly distributed the daily emissions into each hour.

(d) The land–atmosphere carbon fluxes (F_{TA}) are simulated by VEGAS Near-Real Time (VEGAS NRT) (Wang *et al* 2018). The VEGAS NRT was operationally run to present at 0.5° × 0.5° with the automatically updated meteorological fields such as precipitation, surface air temperature, and radiations. The details for the meteorological fields were described in Wang *et al* (2018). In this study, we regarded the difference between F_{TA} and simulated fire emissions (F_{fire}) as 'land–atmosphere carbon flux without fires'.

(e) The ocean-atmosphere carbon fluxes are from Takahashi *et al* (2009) which have been scaled with atmospheric data at 4° × 5° for 2000–2013. We rescaled the oceanic carbon fluxes for the following years using the Global Carbon Project datasets (Friedlingstein *et al* 2019) relative to the year 2013.

2.3. Sensitivity experiments

Two sets of experiments were conducted for the main text, with their experimental designs as follows:

(a) Control experiment (denoted as 'CTL'): full surface carbon emissions considered, including extrapolated ODIAC fossil fuel emissions, extrapolated oceanic carbon exchange, land–atmosphere carbon flux without fires simulated by VEGAS NRT, and GFED4.1 wildfire emissions.

(b) Sensitivity experiment (denoted as 'S1'): same as CTL, but wildfire carbon emissions are set to zero over Australia from November to December 2019.

Thus, we can derive the XCO_2 and 3D CO_2 enhancement caused by the Australian bushfires from the difference between CTL and S1. We ran these two experiments from 1 January 2018 to 31 December 2019 with the CO_2 restart fields from previous long-term simulations.

3. Results

3.1. Australian bushfire carbon emissions and OCO-2 detections

Out-of-control wildfires hit the temperate forests, dominated by fire-prone Eucalyptus, in New South Wales and Victoria from the beginning of November 2019, causing an enhanced amount of carbon (or CO_2) release (figure 1(a)). On average, the carbon release in 0.25° × 0.25° grid from the mega-fires between November and December 2019 is in general higher than 15 gC m^{-2} d^{-1}, in which emissions can reach an extreme of up to 126.9 gC m^{-2} d^{-1} (figure 1(a)). Australia's fossil fuel carbon emissions are also centered over its eastern coastal areas, around the major cities as well as the surrounding power plants (figure 1(b)). It is therefore a concern that fossil fuel emissions may interfere with the space-borne detection of XCO_2 enhancement induced by wildfires. Fortunately, the strength of fossil fuel carbon emissions is found to be much lower than that of the wildfire emissions in these two months. The total fossil fuel carbon emissions in the region of 144–154° E, 40–26° S is approximately 0.2 TgC d^{-1}, leading to a total of 12.2 TgC (or 44.7 $TgCO_2$) for the two months. In contrast, the strength of total wildfire carbon emissions in this region is close to zero before November, and then it becomes much stronger and more variable leading to emissions of approximately 119.0 TgC (or 436.3 $TgCO_2$) during November and December 2019 (figure 1(d)). The wildfire carbon emissions are therefore approximately ten times stronger than fossil fuel emissions in these two months. In addition, the simulated terrestrial ecosystems in this region show a weak absorption (excluding the simulated fire emissions) with the amplitude of 0.08 TgC d^{-1} (figure 1(d)) because November and December are the austral late spring and early summer. Hence, the surface carbon emissions in this region are dominated by the mega-bushfire carbon emissions.

In this region, prevailing winds in the planetary boundary layer are west, west–southwest, and southwest, which blow the emitted CO_2 to the ocean (figure 1(c)). The average wind speed in November and December at 940 hPa is 6.3 m s^{-1}, resulting in about 5.6° longitude advection for 1 d.

We checked the OCO-2 XCO_2 orbit observations around eastern Australia's mega-bushfires between November and December 2019, and selected three orbits that could be used to detect XCO_2 enhancement induced by wildfires. These three orbits were observed at around 03:30 Coordinated Unviersal Time (UTC) on 14 November 2019, 21 November 2019, and 28 December 2019. Figure 2 shows their respective distributions, associated with corresponding wildfire carbon emissions and atmospheric circulation. The XCO_2 values are gradually enhanced from the regions far away from the wildfires to the wildfire downwind areas (figures 2(a)–(c)). These variations are significantly different from the pulse of XCO_2 enhancements induced by the single power plant fossil fuel CO_2 emissions (supplementary figure 2), which is similar to the previous results (Nassar *et al* 2017, Zheng *et al* 2020). Taking the XCO_2 values furthest from the wildfires as the background levels, we used the available XCO_2 values over the fringe areas of plumes to calculate maximum XCO_2 enhancement in these three orbits with their respective

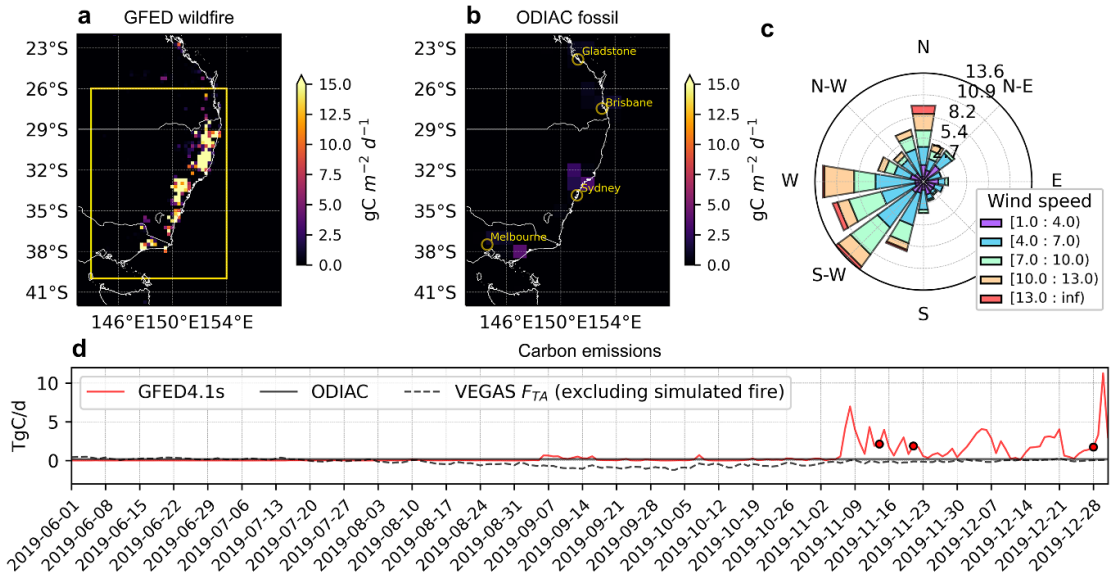

Figure 1. Carbon release by wildfires and fossil fuels. (a) Carbon emissions induced by mega-bushfires, averaged from November to December 2019. (b) ODIAC fossil fuel carbon releases, averaged from November to December 2018. Due to the unavailability of 2019 datasets, we here show data from 2018; the changes in fossil fuel carbon releases over Australia between 2018 and 2019 are likely to be negligible. The unit in (a) and (b) is gC m^{-2} d^{-1}. The rectangular box in (b) shows the area where we calculate the prevailing wind and total carbon emissions. (c) Wind rose diagram at 940 hPa. (d) Total daily carbon fluxes by fossil fuel, mega-bushfires, and terrestrial ecosystems. The dots in (d) show the dates of clear OCO-2 orbit XCO_2 observations.

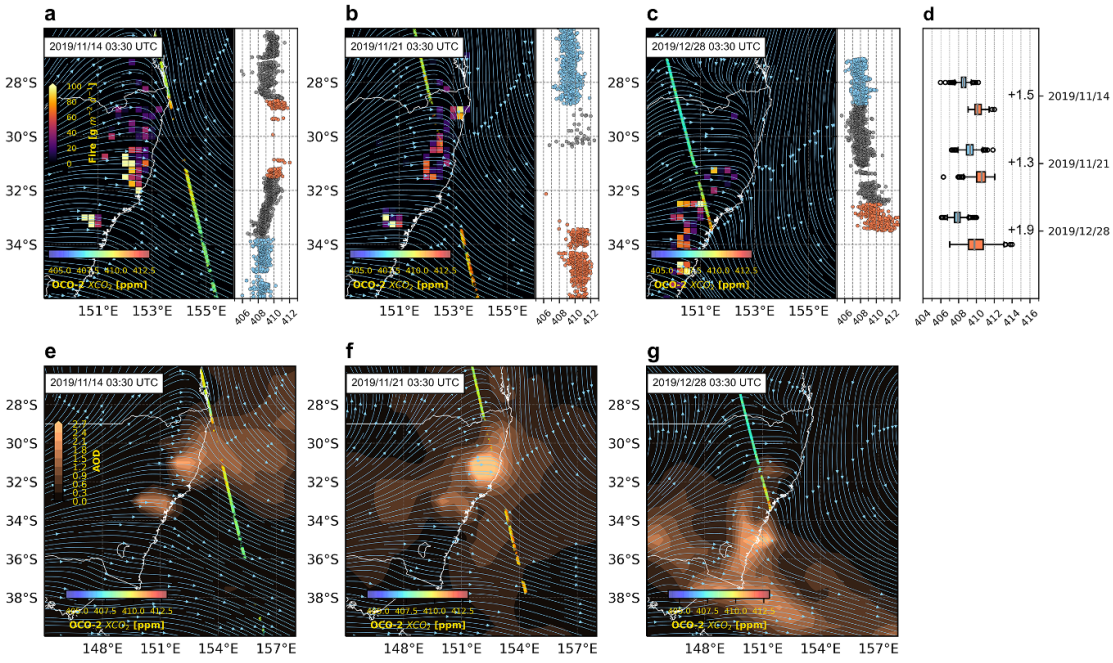

Figure 2. Clear OCO-2 XCO_2 observations at three orbits downwind of the Australian mega-bushfires associated with the corresponding spatial patterns of wildfire carbon emissions, AOD, and stream fields at 940 hPa. The OCO-2 XCO_2 observations at 03:30 UTC with the 24 h averaged wildfire carbon emissions and stream fields before 03:30 UTC on (a) 14 November 2019, (b) 21 November 2019, and (c) 28 December 2019. The scatter plots at the right in (a)–(c) show XCO_2 variation along the latitudes. According to the AOD and simulated XCO_2 (see next figure) patterns, we choose the XCO_2 data far away from the fires to calculate background XCO_2 levels (blue dots here) and data over the fringes of plumes (coral dots) to calculate XCO_2 enhancement against background XCO_2. (d) Box plots for background XCO_2 levels and enhanced XCO_2 for the three orbits. (e)–(g) as (a)–(c), but with the spatial patterns of AOD.

enhancements of approximately 1.5, 1.3, and 1.9 ppm (figure 2(d)).

It is worth mentioning that the gaps of XCO_2 in these three orbits over the wildfire downwind areas are mainly obscured by the amount of smoke emitted by the wildfires. This smoke can enhance the AOD at the local and downwind regions (figures 2(e)–(g)). The local AOD can be higher than 2.7, greatly

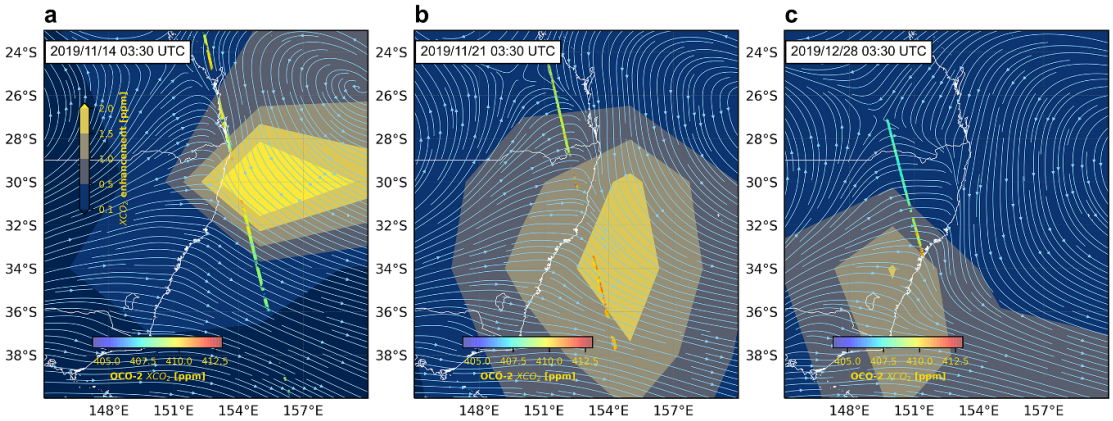

Figure 3. Spatial patterns for XCO_2 enhancement, simulated by the GEOS-Chem model. Simulations at approximately 03:30 UTC on (a) 14 November 2019, (b) 21 November 2019, (c) 28 December 2019. The clear XCO_2 orbits on these 3 d as observed by OCO-2 are also plotted in each figure.

contaminating the OCO-2 XCO_2 observations. The missed observations were often located in the core wildfire-induced XCO_2 enhancement regions, probably leading to an underestimate of the maximum XCO_2 enhancement.

3.2. GEOS-Chem model simulations

The observed XCO_2 variations can be influenced by surface carbon emissions and atmospheric circulation. To further verify that the XCO_2 enhancement observed from the three orbits was caused by wildfire CO_2 emissions, we use the GEOS-Chem model to disentangle the wildfire-induced XCO_2 enhancement with sensitivity experiments (figure 3).

The simulated XCO_2 during November and December in the control experiment has similar spatial patterns and amplitudes compared with OCO-2 observations, although the simulated XCO_2 is approximately 1 ppm higher than results from OCO-2 (supplementary figure 3). In combination with the sensitivity experiment that sets the wildfire carbon flux over Australia as zero emissions during November and December 2019, we can derive the wildfire-induced atmospheric CO_2 variations. Figure 3 shows the spatial patterns for simulated XCO_2 enhancement at around 03:30 UTC on 14 November 2019, 21 November 2019, and 28 December 2019. The higher XCO_2 values from these three orbits observed by OCO-2 coincide with distributions of the simulated XCO_2 enhancement. Importantly, the simulated XCO_2 enhancements are basically comparable to the XCO_2 enhancements detected by OCO-2 (figure 2(d)), confirming that these directly detected XCO_2 enhancements are caused by wildfires. The wildfire CO_2 emissions can also greatly enhance surface CO_2 concentration (supplementary figure 4). From the height–longitude cross-section, we can see that significantly enhanced CO_2 concentrated under 1 km height, and that the enhanced CO_2 in the free atmosphere will be quickly advected (supplementary figure 5).

The sensitivity of XCO_2 maximum enhancement to the wildfire carbon emissions is presented in figure 4. The wildfire carbon emissions were calculated as the total emissions in the region of 144–154° E, 40–26° S (box in figure 1(a)) in the 24 h before 03:30 UTC each day; the XCO_2 maximum enhancement is the average of the simulated XCO_2 values at 03:30 UTC higher than 90th percentile in the region of 145–160° E, 40–26° S. Regression analysis suggests that 1 TgC d^{-1} of wildfire carbon emissions can lead to 0.41 $\pm$ 0.04 ppm XCO_2 maximum enhancement with the R^2 of 0.63 ($P < 0.01$). The relationship between the directly calculated XCO_2 maximum enhancements from OCO-2 orbits and wildfire carbon emissions is also consistent with the simulated relationship.

4. Discussion

Although we have used GEOS-Chem model to verify that the OCO-2 XCO_2 enhancements observed at these three orbits are very likely induced by wildfire CO_2 emissions, one concern is the effect of the uncertainties of the OCO-2 data. Worden *et al* (2017) suggested that effects of aerosols or surface albedo can influence the accuracy of XCO_2 data. Therefore, we present the respective XCO_2 uncertainties at these three orbits in supplementary figure 6. The XCO_2 at 03:30 UTC on 21 November 2019 shows higher uncertainties with values approximately 0.6–0.8 ppm (supplementary figure 6(b)), while the uncertainties at the other two orbits show smaller values approximately 0.4–0.6 ppm (supplementary figures 6(a) and (c)). Indeed, aerosols emitted by wildfires can increase the uncertainties at some pixels, but majorities of the uncertainties are smaller than 0.8 ppm. Therefore, it is convincing that the approximately 1.5 ppm XCO_2 enhancements downwind of the

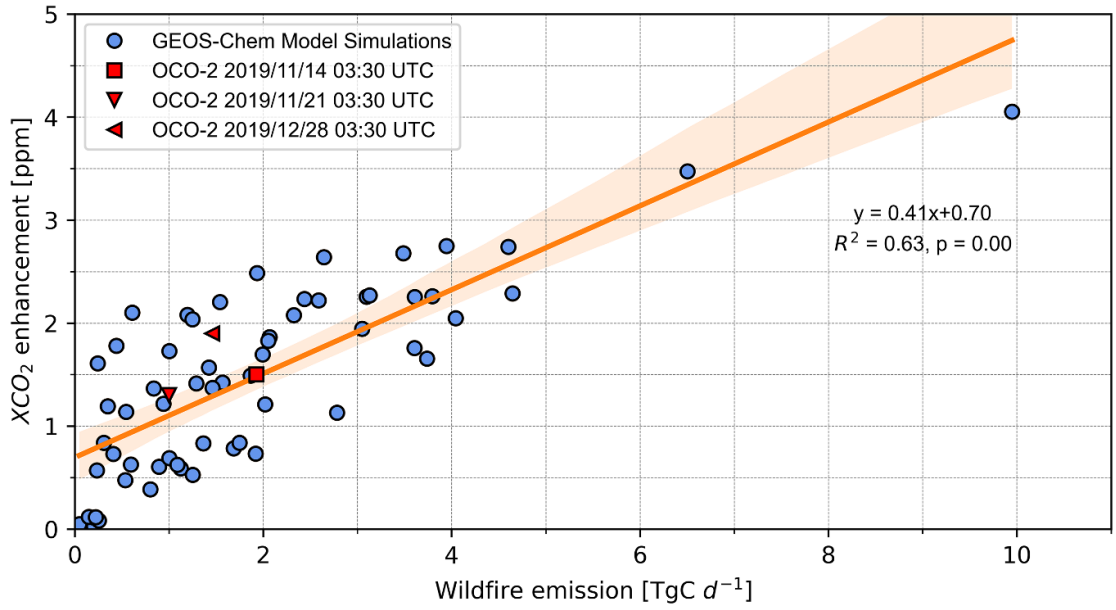

Figure 4. Relationship between XCO_2 maximum enhancement at 03:30 UTC and the preceding 24 h of wildfire carbon emissions. The XCO_2 maximum enhancement in the model simulation is defined as the average of the simulated XCO_2 values higher than the 90th percentile in the domain of 145–160° E, 40–26° S. The orange line represents the linear regression. The OCO-2 observed XCO_2 maximum enhancements from the three different orbits are plotted in red.

major mega-bushfires in eastern Australia at the three orbits cannot be caused by the variations of retrieval uncertainties.

Additionally, we ran two extra sensitivity experiments (supplementary text 2) to explore the influence of carbon flux anomalies induced by the ecosystem and wildfires on the XCO_2 variations. We found that the XCO_2 can be significantly enhanced over the southeast regions of Australia and surrounding oceans by wildfire anomalies in November and December 2019, whereas the enhanced XCO_2 induced by ecosystem carbon anomalies without fires occurs over the northwest regions of Australia (supplementary figure 7). The amplitudes of XCO_2 anomalies induced by wildfire anomalies peak at approximately 0.45 ppm. We also calculated the OCO-2 XCO_2 anomalies based on the method of Chatterjee *et al* (2017). Compared with the simulated amplitudes of XCO_2 anomalies over the southeast regions of Australia and surrounding oceans (supplementary figure 7(d)), the OCO-2 XCO_2 anomalies significantly underestimate the amplitudes over the corresponding regions (supplementary figure 8(a)). This phenomenon is largely caused by smoke contamination from wildfires, which can lead to higher AOD (supplementary figure 8(b)). In addition, the pattern of OCO-2 XCO_2 anomalies contains other information that makes it hard to clarify the influence of eastern Australia's mega-bushfires. Therefore, it is hard to explore the anomalous XCO_2 variations as in the previous study that investigated the anomalous XCO_2 variations caused by the extreme El Niño (Chatterjee *et al* 2017).

5. Conclusions

Base on the NASA OCO-2 XCO_2 product, we in this study investigated whether the recent satellite observations can detect the XCO_2 enhancement induced by the Australian mega-bushfires in November–December 2019. We picked out three orbits downwind of the mega-bushfires in eastern Australia. Though the XCO_2 values at these three orbits exhibit the gradual increase from the regions furthest from the wildfires to the wildfire downwind areas, the XCO_2 values in the core wildfire-induced XCO_2 enhancement regions are obscured by the amount of smoke, making the spaceborne detection challenging. We suggest the approximately 1.5 ppm XCO_2 enhancements at these three orbits, calculating from the difference of available XCO_2 values over outer fringes of plumes and XCO_2 values furthest from the wildfires. This fire-induced XCO_2 enhancement was further confirmed by GEOS-Chem simulations. Based on the simulated results, we point out that the sensitivity of the downwind maximum XCO_2 enhancement is 0.41 ± 0.04 ppm with 1 TgC d^{-1} fire emissions in the region of 144–154° E, 40–26° S.

Acknowledgments

We gratefully acknowledge the OCO-2 project at the Jet Propulsion Laboratory, California Institute of Technology, and obtained from the OCO-2 data archive maintained at the NASA Goddard Earth Science Data and Information Services Center. This

study was supported by the National Natural Science Foundation of China (Grant No. 41807434), the National Key R&D Program of China (Grant Nos. 2016YFA0600204 and 2017YFB0504000). NZ's participation was supported by Grant Nos. NOAA-NA18OAR4310266, NASA-80NSSC18K0908, and NIST-70NANB14H333. Jun Wang (Grant No. 201906195014) thank the China Scholarship Council for funding. The work was conducted while J W was a visiting scientist at the University of Maryland, whose hosting is gratefully acknowledged. We are grateful to the High Performance Computing Center (HPCC) of Nanjing University for doing the numerical calculations on its blade cluster system.

Data availability

All datasets used in this study are publicly available. The OCO-2 L2 products can be accessed at https://oco2.gesdisc.eosdis.nasa.gov/data/OCO2_DATA/OCO2_L2_Lite_FP.9r/; ODIAC fossil fuel emissions are from http://db.cger.nies.go.jp/dataset/ODIAC/; GFED4.1 wildfire emissions are from https://www.geo.vu.nl/~gwerf/GFED/GFED4/; MERRA-2 reanalysis datasets are available at https://gmao.gsfc.nasa.gov/reanalysis/MERRA-2/; TRMM 3B43 precipitation is available at https://disc.gsfc.nasa.gov/datasets/TRMM_3B43_7/summary; SPEI dataset is available at https://spei.csic.es/index.html.

All data that support the findings of this study are included within the article (and any supplementary information files).

ORCID iDs

Jun Wang https://orcid.org/0000-0001-7359-1647
Zhiqiang Liu https://orcid.org/0000-0003-2982-8381

References

Boer M M, de Dios V R and Bradstock R A 2020 Unprecedented burn area of Australian mega forest fires *Nat. Clim. Change* **10** 171–2

Cai W, Cowan T and Raupach M 2009 Positive Indian Ocean Dipole events precondition southeast Australia bushfires *Geophys. Res. Lett.* **36** L19710

Chatterjee A *et al* 2017 Influence of El Nino on atmospheric CO_2 over the tropical Pacific Ocean: findings from NASA's OCO-2 mission *Science* **358** eaam5776

Crisp D *et al* 2012 The ACOS CO2 retrieval algorithm—part II: global XCO2 data characterization *Atmos. Meas. Tech.* **5** 687–707

Crisp D, Miller C E and Decola P L 2008 NASA Orbiting Carbon Observatory: measuring the column averaged carbon dioxide mole fraction from space *J. Appl. Remote Sens.* **2** 023508

Crisp D and OCO-2 Team 2015 Measuring atmospheric carbon dioxide from space with the Orbiting Carbon Observatory-2 (OCO-2) *Proc. SPIE* **9607** 960702

Friedlingstein P *et al* 2019 Global carbon budget 2019 *Earth Syst. Sci. Data* **11** 1783–838

Gelaro R *et al* 2017 The Modern-Era Retrospective Analysis for Research and Applications, version 2 (MERRA-2) *J. Clim.* **30** 5419–54

Heymann J, Reuter M, Buchwitz M, Schneising O, Bovensmann H, Burrows J P, Massart S, Kaiser J W and Crisp D 2017 CO_2 emission of Indonesian fires in 2015 estimated from satellite-derived atmospheric CO_2 concentrations *Geophys. Res. Lett.* **44** 1537–44

Kooyma R M, Watson J and Wilf P 2020 Protect Australia's Gondwana Rainforests *Science* **367** 1083

Liu J *et al* 2017 Contrasting carbon cycle responses of the tropical continents to the 2015–2016 El Nino *Science* **358** eaam5690

Mu M *et al* 2011 Daily and 3-hourly variability in global fire emissions and consequences for atmospheric model predictions of carbon monoxide *J. Geophys. Res. Atmos.* **116** D24303

Nassar R, Hill T G, Mclinden C A, Wunch D, Jones D B A and Crisp D 2017 Quantifying CO_2 emissions from individual power plants from space *Geophys. Res. Lett.* **44** 10045–53

Nolan R H, Boer M M, Collins L, de Dios V R, Clarke H, Jenkins M, Kenny B and Bradstock R A 2020 Causes and consequences of eastern Australia's 2019–20 season of mega-fires *Glob. Change Biol.* **26** 1039–41

O'Dell C W *et al* 2012 The ACOS CO_2 retrieval algorithm—part 1: description and validation against synthetic observations *Atmos. Meas. Tech.* **5** 99–121

Oda T and Maksyutov S 2011 A very high-resolution (1 km × 1 km) global fossil fuel CO_2 emission inventory derived using a point source database and satellite observations of nighttime lights *Atmos. Chem. Phys.* **11** 543–56

Oda T, Maksyutov S and Andres R J 2018 The Open-source Data Inventory for Anthropogenic CO_2, version. 2016. (ODIAC2016): a global monthly fossil fuel CO_2 gridded emissions data product for tracer transport simulations and surface flux inversions *Earth Syst. Sci. Data* **10** 87–107

Phillips N and Nogrady B 2020 The race to decipher how climate change influenced Australia's record fires *Nature* **577** 610–2

Saji N H, Goswami B N, Vinayachandran P N and Yamagata T 1999 A dipole mode in the tropical Indian Ocean *Nature* **401** 360–3

Saji N H and Yamagata T 2003 Possible impacts of Indian Ocean Dipole mode events on global climate *Clim. Res.* **25** 151–69

Schwandner F M *et al* 2017 Spaceborne detection of localized carbon dioxide sources *Science* **358** eaam5782

Takahashi T *et al* 2009 Climatological mean and decadal change in surface ocean pCO_2, and net sea–air CO_2 flux over the global oceans *Deep-Sea Res.* II **56** 554–77

The International GEOS-Chem User Community 2019 geochem/geos-chem: GEOS-Chem 12.5.0 (Version 12.5.0) (Zenodo) (http://doi.org/10.5281/zenodo.3403111)

van der Werf G R *et al* 2017 Global fire emissions estimates during 1997–2016 *Earth Syst. Sci. Data* **9** 697–720

Wang J, Zeng N, Wang M, Jiang F, Wang H and Jiang Z 2018 Contrasting terrestrial carbon cycle responses to the 1997/98 and 2015/16 extreme El Niño events *Earth Syst. Dyn.* **9** 1–14

Worden J R, Doran G, Kulawik S, Eldering A, Crisp D, Frankenberg C, O'Dell C and Bowman K 2017 Evaluation and attribution of OCO-2 XCO_2 uncertainties *Atmos. Meas. Tech.* **10** 2759–71

Zheng B, Chevallier F, Ciais P, Broquet G, Wang Y, Lian J and Zhao Y 2020 Observing carbon dioxide emissions over China's cities with the Orbiting Carbon Observatory-2 *Atmos. Chem. Phys.* **20** 8501–10